The circum-Antarctic ice-shelves respond to a more positive Southern Annular Mode with regionally varied melting

Deborah Verfaillie, Charles Pelletier, Hugues Goosse, Nicolas C Jourdain, Christopher Y. S. Bull, Quentin Dalaiden, Vincent Favier, Thierry Fichefet, Jonathan D Wille

communications earth & environment

ARTICLE

https://doi.org/10.1038/s43247-022-00458-x OPEN

The circum-Antarctic ice-shelves respond to a more positive Southern Annular Mode with regionally varied melting

Deborah Verfaillie[1,4✉], Charles Pelletier[1], Hugues Goosse[1], Nicolas C. Jourdain[2], Christopher Y. S. Bull[3], Quentin Dalaiden[1], Vincent Favier[2], Thierry Fichefet[1] & Jonathan D. Wille[2]

The Southern Hemisphere cryosphere has recently shown regionally-contrasted responses to climate change, in particular to the positive phases of the Southern Annular Mode. However, the understanding of the impacts of this mode on ice-shelf basal melt at a circum-Antarctic scale is still limited. Here, we performed idealized experiments with a pan-Antarctic regional ice-shelf cavity-resolving ocean—sea-ice model for different phases of the Southern Annular Mode. We show that positive phases lead to increased upwelling and subsurface ocean temperature and salinity close to ice shelves, while the opposite occurs for negative phases. A one-standard-deviation increase of the Southern Annular Mode leads to a net basal mass loss of 40 Gt yr^{-1}, with strong regional contrasts: increased ice-shelf basal melt in the Bellingshausen and Western Pacific sectors and the opposite response in the Amundsen sector. Estimates of 1000–1200 and 2090–2100 ice-shelf basal melt changes due to the Southern Annular Mode are −86.6 Gt yr^{-1} and 55.0 to 164.9 Gt yr^{-1}, respectively, compared to the present.

[1] Earth and Life Institute, Université catholique de Louvain, Louvain-la-Neuve, Belgium. [2] Univ. Grenoble Alpes/CNRS/IRD/G-INP, IGE, Grenoble, France. [3] Department of Geography and Environmental Sciences, Northumbria University, Newcastle Upon Tyne, UK. [4] Present address: Aix Marseille Univ., CNRS, IRD, INRAE, CEREGE, Aix-en-Provence, France. ✉email: deborah.verfaillie@gmail.com

The climate of the polar regions has experienced dramatic changes over the past decades[1,2]. The spatial patterns of these changes were regionally contrasted, resulting in heterogeneous impacts on the cryosphere in the Southern Hemisphere. For instance, recent ice sheet mass balance (i.e., the difference between ingoing and outgoing mass fluxes) in Antarctica since the satellite era[3,4] reflects a contrasting west-east dipole in ice losses, as well as in the thinning and weakening of ice shelves (i.e., the floating extensions of the grounded ice sheet) and emissary glacier tongues[5–8]. Furthermore, over the same period, some regions have experienced sea-ice advance, as in the Ross Sea, while other regions such as the Bellingshausen Sea have displayed sea-ice loss[2,9,10]. Recent advances in observing and modeling the Antarctic climate have highlighted both oceanic and atmospheric causes of these trends[7,11–14], with their interactions playing a crucial role. The climate of this region is thus characterized by large internal variability[6,7,15–19]. As a result, no clear consensus appears today on the leading processes controlling changes in the cryosphere in and around Antarctica.

One of the most prominent climate variations during the last century in the high latitudes of the Southern Hemisphere[18] was the millennium-scale maximum in the Southern Annular Mode (SAM)[20,21]. The SAM is the leading principal component of sea level pressure and geopotential height fields in the extratropical Southern Hemisphere[22]. SAM changes are frequently used to explain variations in the near-surface wind speed, air temperature, and precipitation. During phases with a positive SAM, lower sea level pressure at high latitudes and higher sea level pressure at mid latitudes occur, resulting in a stronger pressure gradient and intensified Westerlies, in concert with a southward shift of the Westerlies belt[11,20,23–26]. However, the current knowledge of the impact of these SAM-related fluctuations on the Antarctic cryosphere is still limited. Over the past few years, studies have shown the regionally-contrasted impact of the SAM and the Westerlies on the Antarctic sea ice[27–32] and the surface mass balance of the ice sheet[33–35]. Others have focused on the local impact on coastal ocean warming or ice-shelf basal melt in various Antarctic regions[36–39].

Due to the increasingly positive SAM conditions since the 1950s, driven by stratospheric ozone depletion and increasing greenhouse gases[20,21,25,40], an intensification and poleward shift of the Westerlies has been observed[41–43]. Climate models suggest that this will continue through the rest of the 21st century[26,42,44–46] as dampening effects from the ozone hole recovery will progressively be superseded by increasing effects from greenhouse gas emissions[1,11,47,48]. Spence et al. (2014)[36] and Lin & Wang (2018)[39] showed that this mechanism is expected in turn to drive subsurface ocean warming along the Antarctic coast through changes in Ekman pumping, uplift of the coastal thermocline and increased ice-shelf basal melt. This finding that the impact of the SAM on ice-shelf basal melt is mostly conveyed through mechanic (i.e., surface stress) rather than thermodynamic (i.e., heat fluxes) changes was further refined. Indeed, subsequent studies have reported a significant interplay of ocean circulation and ice-shelf basal melt in the Amundsen Sea[37], in addition to the importance of coastal oceanic waves propagating along the entire Antarctic coastline[38,49]. However, ice-shelf cavities are not always explicitly resolved in the aforementioned modeling studies. This feature is nonetheless key to account for feedback between ice-shelf basal melt and the ocean (e.g., Timmerman et al., 2002, 2012[50,51]; Donat-Magnin et al., 2017[37]; Mathiot et al., 2017[52]; Storkey et al., 2018[53]; Jeong et al., 2020[54]; Richter et al., 2020[55]). Furthermore, to our knowledge, there is no study explicitly linking ice-shelf basal melt to the SAM at the circum-Antarctic scale, impeding the characterization of the potential role of contrasted sub-surface water warming on the sea-ice and ice-sheet mass balance variations at the continental scale. Such a study could allow us to quantify the role of the SAM on the ice-shelf basal melt and the subsequent changes in buttressing of the upstream glaciers (e.g., Reese et al., 2018[56]). This would shed light on the impact of the SAM on the Antarctic ice sheet (AIS) mass balance, which is critical for future global sea-level rise.

In this study, we assess the impact of the SAM on ice-shelf basal melt around Antarctica and the related mechanisms. We further check the response time of ice shelves to a SAM perturbation. To this end, we perform experiments with a cavity-including[52] circum-Antarctic sea-ice–ocean model[57,58], forced by typical SAM perturbations. We quantify the amount of ice-shelf basal melt due to positive and negative SAM perturbations, discuss the various processes at play and the potential reasons for the regionally-contrasted response of ice-shelf basal melt to the SAM. We then present some estimates of ice-shelf basal melt rate changes for different periods in the past and the future. This study thus provides insights into how previously documented mechanisms of ice-shelf basal melt manifest in different regions of Antarctica, as well as the role of feedbacks from ice shelves on the circumpolar climate, and their potential contribution to the recently observed changes.

Results and discussion

What are the impacts of the Southern Annular Mode on ice-shelf basal melt? A positive SAM perturbation (SAM^+ run, corresponding to an increase in the SAM index of one standard deviation, see Methods) yields a net increase in Antarctic ice-shelf basal melt rates. The average ice-shelf basal melt rate change for the perturbed run amounts to 40.3 Gt yr^{-1} for all the ice shelves (thus a statistically significant ~4.1% change compared to the unperturbed annual mean ice-shelf basal melt rate, Table 1). To contextualize this ice-shelf basal melt rate change, we note that it is about half the net accumulation increase over the grounded AIS between 1979 and 2000 (78.6 ± 26.5 Gt yr^{-1} relative to the nineteenth-century mean[33]). This could also be put in context of satellite-derived measurements of the rates of the Antarctic ice-sheet mass change over the period 1992–2011 (-76 ± 59 Gt yr^{-1}) and 1992–2017 (-109 ± 56 Gt yr^{-1})[3]. The average ice-shelf basal melt rate change we obtain in Table 1 is also a quarter of the excess ice-shelf meltwater flux over 1994–2018 (160 ± 150 Gt yr^{-1}, compared to steady state), estimated through satellite and firn model data[59]. Even though our SAM idealized experiments are imperfect representations of the real world, they suggest that the

Table 1 Ice-shelf basal melt rate change due to a positive SAM perturbation.

	Mean ice-shelf basal melt rate (Gt yr^{-1})	Ice-shelf basal melt rate change (Gt yr^{-1})	% change (%)
Pan-Antarctic	979.4 ± 0.2	40.3 ± 0.0	4.1 ± 0.0
Ross	63.3 ± 0.0	0.2 ± 0.0	0.3 ± 0.0
Amundsen	372.9 ± 0.6	-39.5 ± 0.1	-10.6 ± 0.0
Bellingshausen	89.7 ± 0.2	44.1 ± 0.1	49.1 ± 0.1
Weddell	159.4 ± 0.1	13.9 ± 0.0	8.7 ± 0.0
Indian Ocean	57.7 ± 0.1	-5.7 ± 0.0	-9.9 ± 0.1
Western Pacific	236.5 ± 0.7	27.3 ± 0.2	11.6 ± 0.0

CTRL mean annual ice-shelf basal melt rate over the 30 year period (Gt yr^{-1}), compared to the mean ice-shelf basal melt rate change between the SAM^+ run and the CTRL run averaged over years 25 to 29 (Gt yr^{-1}), and the corresponding percentage change (%) at the pan-Antarctic scale and for each of the six regions. Ninety-five percent confidence intervals are given. All ice-shelf basal melt rate change values are statistically significant at the 99% level. The regions are defined in Fig. 1.

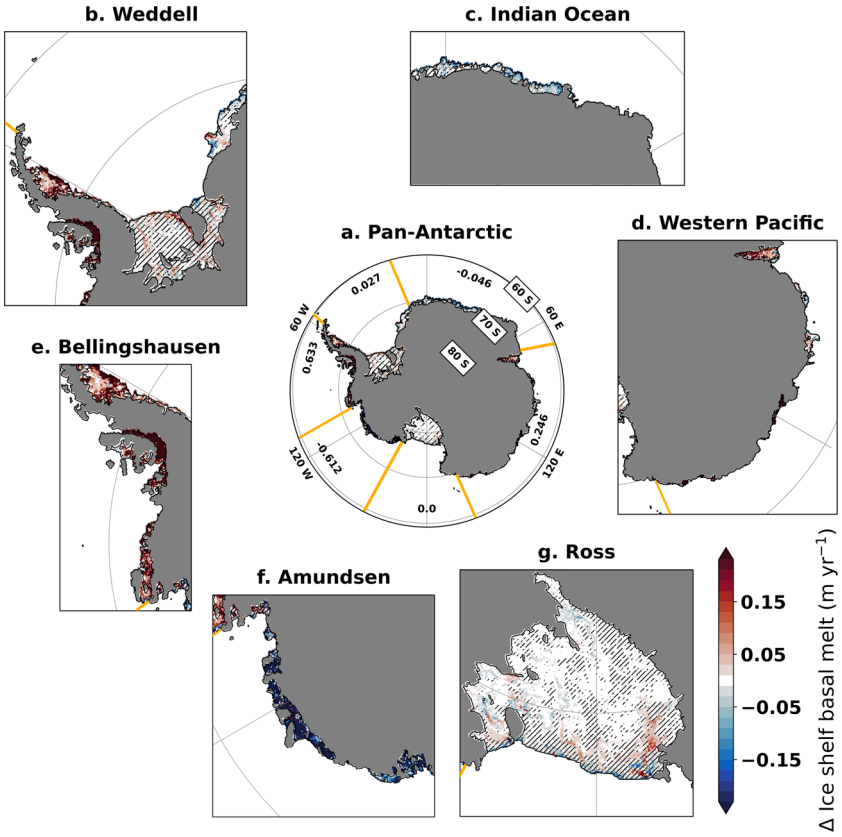

Fig. 1 Spatial variations of ice-shelf basal melt rate change due to a positive SAM perturbation. Maps of the ice-shelf basal melt rate change between the SAM$^+$ run and the CTRL run averaged over years 25 to 29 (m water equivalent yr^{-1}), (**a**) at the pan-Antarctic scale and (**b**–**g**) for each of the six regions delimited by the orange lines in (**a**) (see also Fig. S1). Mean values for each of the six regions are indicated in (**a**). Hatching indicates non-significant changes at the 95% level.

intensification of the SAM could explain about one tenth (−6.4 Gt yr^{-1}), one quarter (−26.5 Gt yr^{-1}) and one fifth (30.7 Gt yr^{-1}) of, respectively, the AIS mass change over 1992–2011, the AIS mass change over 1992–2017 and the excess meltwater flux estimated over 1994–2018 (see "Methods").

The ice-shelf basal melt rate response to increased SAM is positive in all regional averages except for the Amundsen and Indian Ocean regions (~− 10.6% and~−9.9% change, respectively, compared to the unperturbed annual mean ice-shelf basal melt rates, Table 1). The impact on ice-shelf basal melt is strongest on the smaller ice shelves of the Western Pacific (~11.6% change) and Bellingshausen (~49.1% change) sectors, and on the Antarctic Peninsula (Table 1, Fig. 1, Supplementary Table S1, Supplementary Movies S1–S7). Elsewhere, the impact is more contrasted (Fig. 1, Supplementary Movies S1–S7). Ice-shelf refreezing occurring in large, cold cavities (e.g. Filchner-Ronne, Ross[59–62]) occurs more strongly in the SAM$^+$ experiment, suggesting a SAM-related enhancement of the ocean – ice shelf interactions, regardless of its nature (refreezing or melting), which is consistent with the ice pump circulation[63].

The increase in ice-shelf basal melt rate contrasts with the small net increase in annual mean sea-ice extent (~15.5 10^4 km^2, statistically significant at the 95% level, Supplementary Fig. S2) caused by the positive SAM perturbation. On the one hand, compared with other multimodel studies relying on longer coupled experiments[64], this relatively mild impact on the sea-ice cover may be related to the fact that our ocean-standalone simulations cannot account for coupled atmosphere—ocean feedbacks (e.g., related to ozone depletion[65]). Moreover, contrary to global climate models, our eddy-permitting[66]1/4° configuration might harbor eddy compensation[67] which could inhibit the simulated sea-ice reaction, albeit in a lesser extent compared with other modeling studies clearly set over eddy-resolving resolutions[68,69]. On the other hand, this moderate simulated SAM-related sea-ice impact is consistent with several other studies[27,70,71] showing that the SAM cannot explain the Antarctic sea-ice extent increase during the satellite era. Nevertheless, although the impact of the SAM on the total Antarctic sea-ice extent is almost negligible, sea-ice extent changes are also regionally contrasted (Fig. S3). For instance, a positive SAM perturbation leads to a sea-ice extent increase in the Ross and Weddell sectors while the Bellingshausen sector witnesses a slight sea-ice extent decrease (Fig. S3). This spatial pattern typically arises from the atmospheric circulation in West Antarctica associated with the positive SAM conditions, that enhance the southerly warm airflow towards the Antarctic Peninsula and the cold airflow from the ice sheet towards the Ross Sea[24,27,72]. More generally, the fact that the ice-shelf basal melt is much more sensitive to a SAM perturbation than the sea ice indicates a contrasted response between the subsurface and the surface.

When examining ice-shelf response times to SAM perturbations at an Antarctic-wide scale (Fig. 2), the response time is in the order of a decade, except for the Bellingshausen sector that does not reach an equilibrium during our experiment, and the Amundsen and Western Pacific sectors that take nearly 25 years. This is longer than reported, e.g., in Spence et al. (2017)[38], possibly because the residence time of waters below the Ross and Filchner-Ronne ice shelves is very long (several years, e.g. Michel et al., 1979[73]; Nicholls and Osterhus 2004[74]; Naughten et al., 2019[75]), which may enable circum-Antarctic recirculation.

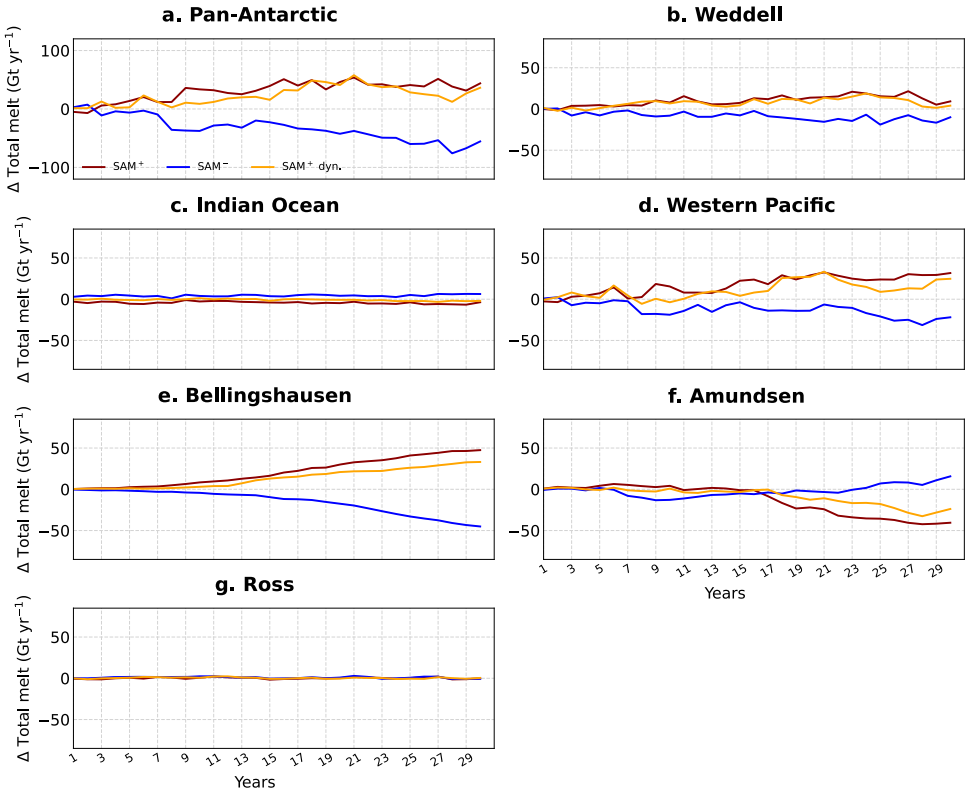

Fig. 2 Evolution of ice-shelf basal melt rate in response to the SAM perturbations. Time series of (**a**) pan-Antarctic and (**b**–**g**) regional ice-shelf basal melt rate change (in Gt yr^{-1}) between the SAM^{+} run and the CTRL run (red line), the SAM^{-} run and the CTRL run (blue line) and the SAM$^{+}_{dyn}$ run and the CTRL run (orange line). The x-axis represents year 1 through 30 of each simulation. The regions are defined in Fig. 1.

However, one should bear in mind the differences in experimental setup between both studies: wind forcing in Spence et al. (2017)[38] was much stronger than ours, and ice shelves were not accounted for. This shows the interest of using a model that covers the whole circum-Antarctic region. The SAM^{+} run first experiences a slight decrease in pan-Antarctic ice-shelf basal melt rate (during the first two years), then an increase, which reaches a plateau after about nine years. This two-time-scale response of ice-shelf basal melt rates to a positive SAM perturbation is similar to the one found by Naughten et al. (2021)[76] in response to climate warming associated with increased CO_2 concentration, although it occurs on shorter time scales in this study. A two-time-scale response of the sea ice to ozone depletion was also found in Ferreira et al. (2015)[77].

The response to a SAM^{-} perturbation (see "Methods") almost mirrors the SAM^{+} one for all sectors but the Amundsen sector where a negative SAM anomaly has no significant effect on ice-shelf basal melt. Melt rates obtained with the run in which only the dynamical components were perturbed (SAM$^{+}_{dyn}$ run, see "Methods") are similar to the ones obtained with the SAM^{+} run, confirming that the ice-shelf response is mostly wind-driven. The Indian Ocean (Fig. 2c) and Ross (Fig. 2g) sectors exhibit very little response to any SAM perturbation, as already reflected in the 5-year averages of Table 1.

What are the processes at play? Sectors that experience the largest ice-shelf basal melt rate increase associated to SAM^{+} (i.e., the Western Pacific and Bellingshausen sectors, Figs. 1, 2) are generally the ones where ice-shelf cavities are in direct contact with warmer-than-usual (warmer-than-CTRL) water masses (Fig. 3, Supplementary Fig. S4). Figure 3 indicates that the whole Antarctic Peninsula undergoes strong warming at the ice-shelf front, in particular the Bellingshausen region and the western side of the Antarctic Peninsula (consistently with previous studies[46,78]). Water masses located above the continental shelf (around 1000 m depth) are warmer than in the CTRL run by ~0.1 °C in the Western Pacific sector (Fig. 4c) and by up to ~0.25 °C in the Bellingshausen sector (Fig. 4d). By comparison, with a rather different experimental design and a regionally-limited forcing, Webb et al. (2019)[49] get a warming along the West Antarctic Peninsula of up to 0.7° C. In contrast, in the Amundsen sector, where SAM^{+} leads to decreased ice-shelf basal melt rates (Figs. 1, 2), water masses above the continental shelf are 0.3 ° C colder than in CTRL (Fig. 4e). Processes explaining this opposite response of the Amundsen sector are discussed later. The Weddell, Ross and Indian Ocean sectors exhibit slightly colder water close to the continent (Fig. 4a, b, f), which is consistent with the modest increase (or decrease in the case of the Indian Ocean) in ice-shelf basal melt rates in these regions (Table 1). However, water masses located off the continental shelf, around 65–70°S, are warmer for most regions, including Amundsen (Fig. 4). In terms of salinity, subsurface water masses get saltier everywhere close to the Antarctic continent, by up to ~0.2 g kg^{-1} in the Ross and Bellingshausen sectors (Figs. 3, 4).

Concerning temporal evolution, subsurface ocean temperature and salinity tend to increase with time (Supplementary Fig. S2), with different response times depending on the sector considered (Supplementary Figs. S4–S7). A maximum temperature difference between the SAM^{+} run and the CTRL run is reached after about nine years for the Indian Ocean (Supplementary Fig. S6b), after about 20 years for the Weddell and Western Pacific sectors (Supplementary Fig. S6a, c), and is never reached even after 30 years of simulation for the Bellingshausen sector (Supplementary Fig. S6d). For this sector, as currently the ice-shelf basal melt has most probably not reached an equilibrium yet, this tends to

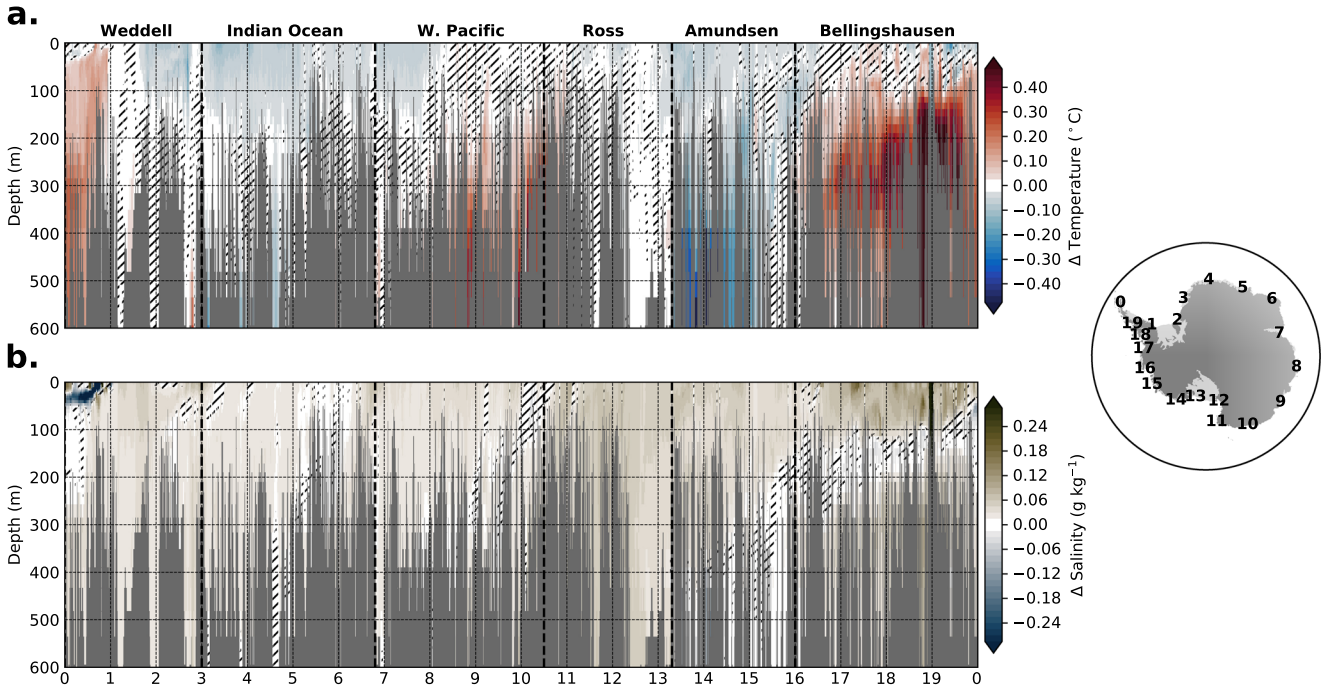

Fig. 3 Ocean conservative temperature and absolute salinity changes at the ice-shelf front due to a positive SAM perturbation. Vertical sections of (**a**) ocean temperature (°C) and (**b**) salinity (g kg^{-1}) changes between the SAM^{+} run and the CTRL run along the ice-shelf front. Values are averaged over years 25–29. Hatching indicates non-significant changes at the 95% level. The bedrock bathymetry is represented in gray. The x-axis represents the position along the ice-shelf front, indicated by numbers from 0 to 19 located on the inset map.

indicate that ice-shelf basal losses should continue to amplify in the future under positive SAM conditions. Ocean temperature and salinity changes under the SAM^{-} perturbation show an opposite evolution (Supplementary Figs. S4, S5).

The intrusion of warmer, saltier water on the continental shelf in the Bellingshausen and Western Pacific sectors as well as the eastern side of the Antarctic Peninsula is due to an increase in upwelling (represented by the maximum vertical velocity, see "Methods") near the shelf break (Fig. 5), which brings warmer and saltier water close to the ice shelves base, thereby increasing ice-shelf basal melt[27,28,36–39]. The circum-Antarctic zonal mean upwelling off the continental shelf break increases by ~ 4.5×10^{-6} m s^{-1} (i.e., ~ 5.2%) in the SAM^{+} and SAM$^{+}_{dyn}$ runs compared to the CTRL run (Fig. 5c, d). This increase in upwelling is induced by the intensification and southward shift of ocean surface stress over the Southern Ocean in response to positive SAM conditions (Fig. 5a, b). Around 55°S, the mean zonal surface stress increases by ~ 0.004 N m^{-2} (i.e., ~ 2.9%) and is shifted poleward by about 0.1° in the SAM^{+} and SAM$^{+}_{dyn}$ runs compared to the CTRL run (the surface stress response to a negative SAM perturbation mirrors the latter response to a positive SAM perturbation). This typical mechanism associated with the intensification and poleward shift of the Westerlies was already described in previous studies[36,37,39]. However, it is noteworthy that in this study, the ice-shelf basal melt response is fairly large (4.1% change at the pan-Antarctic scale and 49.1% change in the Bellingshausen region), despite a rather small surface stress perturbation (0.1° shift and ~2.9% intensity increase). By comparison, using a different experimental design, Spence et al. (2014)[36] applied a 4° shift and 15% stronger winds.

The fact that ice-shelf basal melt rates obtained with the run in which only the dynamical components were perturbed (SAM$^{+}_{dyn}$ run) are similar to the ones obtained with the SAM^{+} run, confirms our hypothesis that the ice-shelf response is mostly wind-driven, conveyed through an intensification and southward shift of ocean surface stress (related to the Westerlies) and subsequent increase in upwelling close to the majority of Antarctic ice shelves. Supplementary Figs. S2a and S3a, b show very little change in sea ice extent in the SAM$^{+}_{dyn}$ run compared to the CTRL run, in contrast with the sea ice response of the SAM^{+} and SAM^{-} runs. This could indicate that sea ice is sensitive to a more complex combination of elements than ice-shelf basal melt, which is mostly driven by the upwelling variations. Our study therefore confirms this mechanistic hypothesis for most regions around Antarctica and goes further in quantifying and explaining the processes responsible for enhanced (reduced) ice-shelf basal melt under positive (negative) SAM conditions.

Why is the response regionally contrasted? All regions (with the exception of Amundsen and the Indian Ocean) exhibit an increase in ice-shelf basal melt in response to a positive SAM perturbation. Moreover, the regions with a positive response still feature distinct patterns. The Ross and Weddell regions exhibit a weak increase in ice-shelf basal melt, both in terms of mean state (Table 1) and temporal evolution (Fig. 2). Smaller ice shelves located in the Western Pacific and Bellingshausen sectors and the Antarctic Peninsula respond more strongly to the perturbation than the larger ones such as Filchner-Ronne and Ross ice shelves (Fig. 1 and Supplementary Table S1). The negative response observed in the Indian Ocean region could be related to a decrease in upwelling in that region (Fig. 5c).

In contrast with the other Antarctic regions, ice-shelf basal melt in the Amundsen sector decreases when a positive SAM perturbation is applied (Table 1, Figs. 1, 2). This decrease is related to a cooling of the subsurface waters above the continental shelf in the Amundsen and eastern Ross seas (Figs. 3, 4 and Supplementary Fig. S6). Holland et al. (2019)[7] and Naughten et al. (2022)[79] suggest the westerly wind trend over the shelf break in the Amundsen region may on the contrary have contributed to a long-term warming signal on the shelf and the on-going ice loss

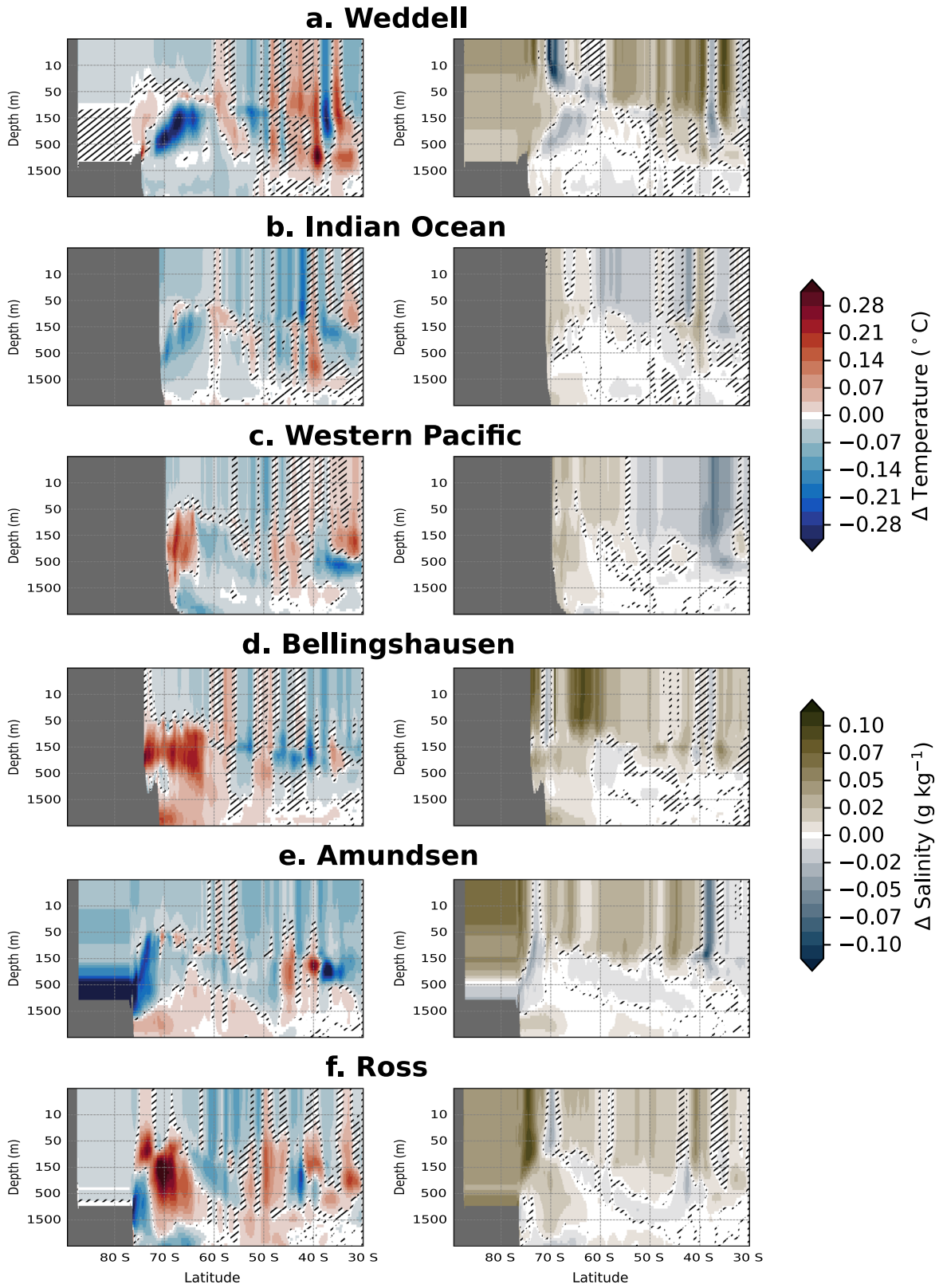

Fig. 4 Zonally-averaged vertical sections of ocean conservative temperature and absolute salinity changes due to a positive SAM perturbation. Depth vs. latitude sections of ocean temperature (°C) and salinity (g kg^{-1}) changes between the SAM^{+} run and the CTRL run for the six regions (**a**–**f**). Values are averaged over years 25–29, and ice-shelf cavity columns are excluded from the zonal averaging. Hatching indicates non-significant changes at the 95% level. The regions are defined in Fig. 1.

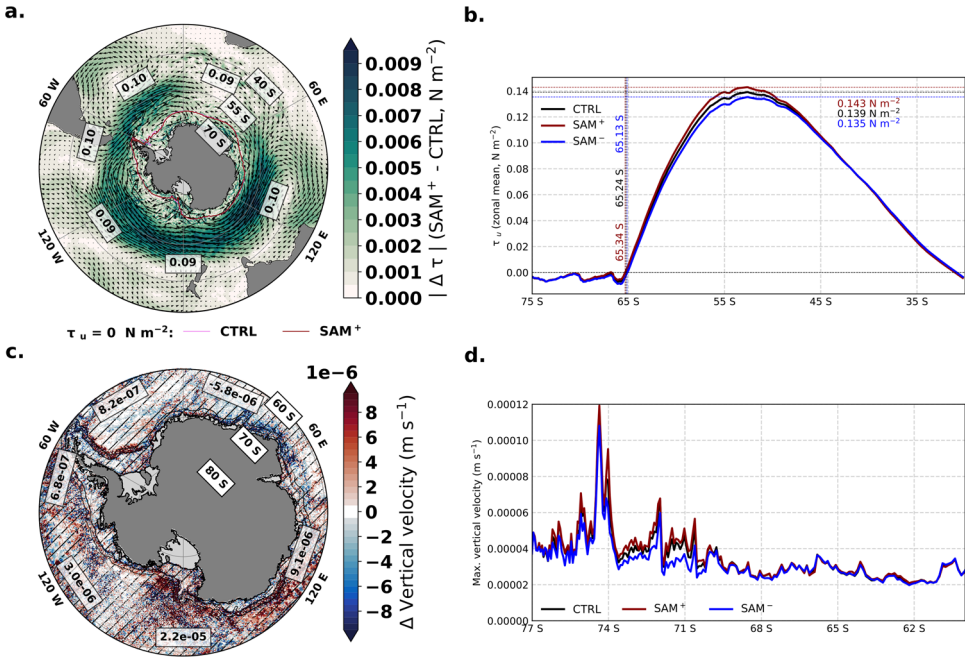

Fig. 5 Impact of SAM perturbations on the ocean. a Shadings: norm of the ocean surface stress difference between the CTRL and SAM$^+$ runs (i.e.,$\| \boldsymbol{\tau}^{SAM^+} - \boldsymbol{\tau}^{CTRL} \|$); the two colored contours indicate zonal surface stress sign changes (i.e. $\tau_u = 0$) for both experiments; text boxes give each sector's average meridional shift in zonal stress direction change (in °; positive values indicate southward shift). **b** Circum-Antarctic zonal mean of the zonal surface stress in the CTRL, SAM$^+$ and SAM$^-$ runs. The SAM^+_{dyn} zonal mean surface stress response is identical to the SAM$^+$ one, so it was not represented here. Colored vertical and horizontal lines, respectively, specify the latitudes of the southward shift of the mean zonal zero surface stress and the maximum westerly surface stress values. Here, "surface stress" is the total stress absorbed by the surface of the ocean, i.e. the combination of wind- and sea-ice-induced surface stresses weighted by the sea-ice concentration. **c** Map of the change in maximum vertical velocity (m s^{-1}, representative of upwelling) between the SAM$^+$ run and the CTRL run. Hatching indicates non-significant changes at the 95% level and mean values (for the region located between the continental shelf break and 100 km north of the continental shelf break, delimited by the dotted lines) for each of the six regions shown in Fig. 1 are indicated inside white boxes. **d** Circum-Antarctic zonal mean maximum vertical velocity in the CTRL, SAM$^+$ and SAM$^-$ runs. The SAM^+_{dyn} zonal mean vertical velocity response is similar to the SAM$^+$ one, so it was not shown here. All values are time-averaged over years 25–29.

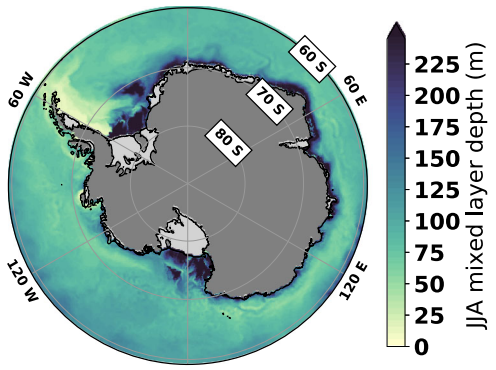

Fig. 6 Winter mixed layer depth in the CTRL run. Map of the winter (JJA) mixed layer depth in the CTRL run. Values are averaged over years 25 to 29.

in this region. Discrepancies between these studies and our findings could be due to the different experimental setups and different definitions of the Amundsen region. Furthermore, in contrast with Holland et al. (2019)[7], we directly assess the response of ice-shelf basal melt rates to a SAM perturbation, and not to changes in the Westerlies, which, in the Amundsen Sea are mostly related to ENSO[7].

The relative cooling in the Amundsen region is in contrast with the large increase in ice-shelf basal melt and subsurface temperatures simulated in the Bellingshausen region. This dipole is potentially a fingerprint of the Amundsen Sea Low (ASL) – a low pressure system centered in the Pacific sector, off the coast of West Antarctica—which is typically deeper during SAM$^+$ conditions[72,80]. A deeper ASL prompts colder, northerly air advected from the Antarctic continent in the eastern Ross region, bringing a decrease in sea surface temperatures along with enhancing the sea-ice concentration[81]. Dotto et al. (2020)[82] further showed that a deep ASL was associated with westward wind anomalies at the continental shelf break in the Amundsen region, resulting in a deceleration of the shelf break undercurrent and a cooling of the Getz-Dotson Trough.

The pattern of increasing sea-ice production and decreasing surface temperature in the Amundsen-eastern Ross region is also generally observed when SAM is positive[27,28,83,84], implying more vertical mixing in the water column (with an increase in the winter mixed layer depth off the eastern Ross ice shelf of about 80 m). Our results suggest that the relationship between SAM and surface temperatures/sea-ice area in the Amundsen-eastern Ross region can be extended to ice-shelf basal melt. The increase in northerly winds during positive phases of the SAM directly implies a cooling of surface waters in the eastern Ross Sea due to colder air advected from the continent (Supplementary Fig. S8), which is transferred to the subsurface through intense vertical mixing (Fig. 6). The cold and saline waters in the Amundsen-eastern Ross Sea (Figs. 3, 4) are consistent with an intensification of sea-ice production in this region[27,28]. The sea-ice production over the Amundsen-eastern Ross continental shelf increases by ~1.5 10^{-4} m day^{-1} in the SAM$^+$ run compared to the CTRL run. Moreover, this region experiences a stronger slope current under positive SAM conditions (Fig. 7), preventing the warmer waters from coming onto the continental

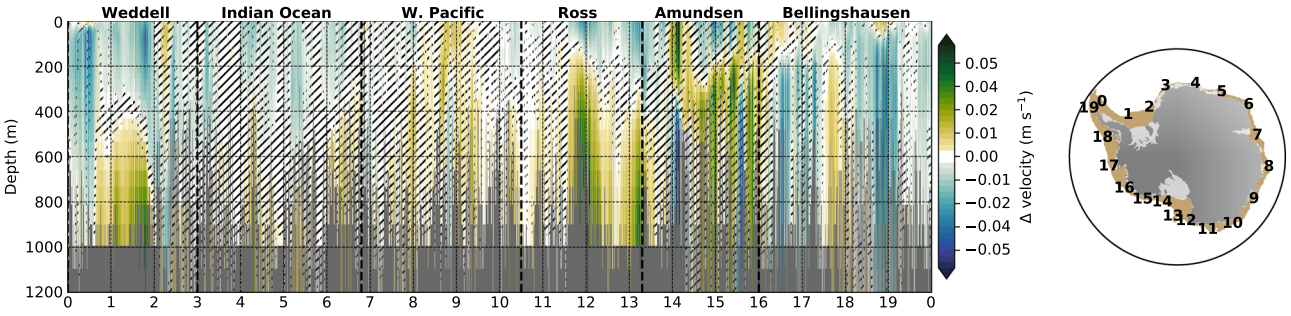

Fig. 7 Slope current velocity change due to a positive SAM perturbation. Vertical section of the geostrophic slope current velocity (defined as the along-slope geostrophic velocity at the continental shelf break[85]) change between the SAM+ run and the CTRL run, averaged over years 25 to 29. The bedrock bathymetry is represented in gray. Hatching indicates non-significant changes at the 95% level. The x-axis represents the position along the shelf break, indicated by numbers from 0 to 19 located on the inset map (the continental shelf is represented in tan).

Table 2 Estimates of ice-shelf basal melt rate changes in the past and future.

	Last millenium[20]	End of the century[26]		
		SSP245/RCP4.5	SSP585	RCP8.5
Period (years AD)	1000–1200	2090–2100	2090–2100	2090–2100
Number of σ SAM	−2.1	1.4	3.3	4.1
Ice-shelf basal melt rate change (Gt yr^{-1})	−86.6	55.0	131.9	164.9

Estimates of the changes in the SAM index (expressed in standard deviations (σ) of the SAM index compared to our reference period 1989–2018) and subsequent changes in pan-Antarctic ice-shelf basal melt rate for different periods in the past and future: the beginning of the last millennium (1000–1200 AD, based on the SAM reconstruction from Abram et al., 2014[20]) and the end of the 21st century (2090–2100, based on SAM index projections from Fig. S3 from Goyal et al., 2021[26]). For end-of-century projections, emission scenarios SSP245/RCP4.5, SSP585 and RCP8.5 are considered.

shelf[85,86]. As a consequence, the water masses above the continental shelf, in contact with the Amundsen and eastern Ross Sea ice-shelves base, are colder-than-usual, thereby reducing ice-shelf basal melt.

Another possible explanation of the regional contrasts in ice-shelf basal melt responses to the SAM could come from the redistribution of ice-shelf meltwater. Nakayama et al. (2014)[87] showed that basal melting of the Amundsen and Bellingshausen ice shelves triggered a freshening of the Ross Sea through increased transport of meltwater to the eastern Ross sector. However, in our study, a positive SAM perturbation leads to saltier water almost everywhere and no freshening of the eastern Ross Sea waters is observed (Figs. 3, 4, Supplementary Fig. S7).

What would be the response of ice-shelf basal melt to past or future SAM variations? To conclude, our study is the first to address the impact of the SAM on ice-shelf basal melt at a circum-Antarctic scale. The study has shown that positive phases of the SAM lead to a net increase in Antarctic ice-shelf basal melt, due to enhanced upwelling transporting warmer and saltier waters to the subsurface close to the ice-shelf base. We thereby confirm the mechanistic hypothesis associated with the intensification and poleward shift of the Westerlies, already described in previous studies. Our study also goes further in explaining in details the mechanisms responsible for enhanced (reduced) ice-shelf basal melt under positive (negative) SAM conditions.

We further show contrasts in the regional response of ice shelves to SAM perturbations, with a positive perturbation leading to increased basal melt in the sectors of the Western Pacific and Bellingshausen, and an opposite response in the Amundsen-eastern Ross Sea sector. We argue that the negative response of the Amundsen sector in the case of a positive SAM perturbation could be related to the interplay between the ASL and the SAM, as well as the presence of colder air advected from the continent over the eastern Ross Sea coupled to more vertical mixing and a stronger slope current preventing warmer waters from reaching the Amundsen and eastern Ross ice-shelves base.

The results of our experiments provide an estimate of the changes induced by a one-standard-deviation change in the SAM index for present-day conditions. Assuming that this response of the system to SAM is stationary, we can compute the impact of past and future SAM changes on ice-shelf basal melt by simply multiplying the value obtained in our experiments by the difference in the SAM index between selected periods and the present day. Based on the SAM reconstruction for the last millennium from Abram et al. (2014)[20], we find that the SAM index at the beginning of the last millennium (1000–1200 AD) was about 2.1 standard deviation lower compared to the 1989–2018 mean SAM index (Table 2). As a consequence, the pan-Antarctic ice-shelf basal melt rate change at the beginning of the last millennium compared to the present is estimated at − 86.6 Gt yr^{-1}. Similarly, using SAM projections from Fig. S3 of Goyal et al. (2021)[26] for the end of the century (2090–2100), we find changes in the SAM index between +1.4 and +4.1 standard deviation compared to the 1989–2018 mean, depending on the emission scenario considered (Table 2). The future pan-Antarctic ice-shelf basal melt rate change due to the SAM at the end of the century can thus be estimated between 55.0 and 164.9 Gt yr^{-1} compared to the present. This is much smaller than the total expected end-of-century change in basal melt rates from, e.g., Golledge et al. (2019)[88] or Timmermann & Hellmer (2013)[89].

While the estimates described herein are statistically robust and indicate the potentially important impact of the SAM on the AIS mass balance, other unrepresented processes impacting ice shelves provide leads for future likewise circum-Antarctic studies. For example, our study does not account for feedbacks related to the evolution of ice-sheet geometry (through melting, surface

mass balance or iceberg calving anomalies), which could trigger substantially important destabilization through marine ice-sheet and ice-cliff instabilities. Another perspective lies in investigating the impact of other modes of Southern climate variability on ice shelf—ocean interactions such as the El Niño Southern Oscillation (ENSO). Our idealized experimental design permitted clearly identifying and isolating SAM-related effects on such interactions, but the contrasted (both sector and process-wise) response of the Antarctic cryosphere presented above suggests that the physics at play cannot be interpreted uniformly and unequivocally. In particular, investigating the joint impact of SAM- and ENSO-related processes on ice-shelf cavities remains a considerable challenge, as the response of the cryosphere to such climate fluctuations may be more complex than the superposition of the responses to each of them taken separately.

Methods

Model setup. The model used in this study is the ocean—sea-ice model NEMO v.3.6 (Nucleus for European Modeling of the Ocean[58])—LIM3.6 (Louvain-la-Neuve sea-ice model[57]), including the explicit ice-shelf cavity module[52]. The model is used in a standalone setup, i.e., without coupling nor feedback with the atmosphere or dynamical ice sheet. The model grid (ePERIANT025) has a ~ 0.25° resolution in longitude and covers the Antarctic ice shelves[52], the circum-Antarctic seas and the Southern Ocean, with one single lateral boundary at 30°S. The configuration is derived from the GO7 one described in Storkey et al. (2018)[53]. The ocean model horizontal resolution increases from 24 km at 30°S to 3.8 km at ~86°S. A so-called $z^\star$ coordinate is employed, with 75 vertical levels whose thicknesses increase from 1 m at the surface to ~200 m at depth, so that the vertical resolution at the ice shelf—ocean interface ranges from ~10 to ~150 m. The NEMO and LIM time steps are 900 s and 5400 s, respectively. The Antarctic continental shelf bedrock bathymetry is taken from the Nov. 2019 version of BedMachine Antarctica[90], and a linear transition to ETOPO1[91,92] is performed north of ~63°S. The Antarctic ice-sheet geometry, from which the surface continental mask is derived, is constant and taken from a relaxation run performed with the f.ETISh ice-sheet model at 8 km resolution[93]. Ice-shelf cavities are explicitly resolved[52] with ocean–ice-shelf heat and freshwater fluxes parameterized from the intra-cavity ocean circulation as in Pelletier et al. (2022)[94]. Antarctic ice-sheet calving is not represented, but iceberg melting is represented as additional runoff with associated increased near-surface mixing[12,95]. No sea surface salinity restoring is applied. At the ocean surface, the model is forced at a 3-hourly frequency with air-sea fluxes derived from the CORE bulk formula[96], using a normal year from ERA5[97] as atmospheric input. The normal year (i.e., most neutral in terms of major climate modes of variability) of Stewart et al. (2020)[98] is used, by repeating the ERA5 forcing from 1st May 1990 to 30th April 1991. At its northern lateral boundary (30°S), the model is relaxed to the ORAS5 ocean reanalysis[99].

Experiments. Four experiments were performed with the NEMO-LIM3.6 model. The control experiment (CTRL) corresponds to the baseline experiment against which SAM-perturbed experiments are compared. It is a 40-year long NEMO-LIM3.6 run forced by the normal-year ERA5 forcing described above (with ocean initial conditions taken from a previous NEMO standalone run). Three additional 30-year long SAM-perturbed experiments were then produced: SAM^+, SAM^- and SAM^+_{dyn}. For each of those, a seasonal SAM perturbation - corresponding to changes representative of an increase or a decrease in the SAM index of one standard deviation - was added to or substracted from the CTRL forcing for all the variables used to force the model (surface specific humidity, total precipitation, snowfall, surface thermal and solar radiation downwards, 2 m temperature, 10 m u- and v-wind speed) or for only some of them. To calculate the SAM^+ and SAM^- perturbations of a variable x for a given timestep, we calculate the regression coefficient between x (from ERA5 over 1989–2018) and the non-dimensional SAM index (index divided by its standard deviation) timeseries of the corresponding season. For SAM^+ (SAM^-), the SAM perturbation was added to (subtracted from) all the forcing variables, while for SAM^+_{dyn}, only the dynamical components (surface u- and v-wind speed) were perturbed. The SAM^+_{dyn} perturbation thus impacts surface stress but also turbulent heat fluxes, i.e. we also expect changes in sea ice production, not only Ekman pumping. Each SAM-perturbed run was restarted from the CTRL run after 10 years.

Pan-Antarctic and regional diagnostics. All diagnostics were performed at the pan-Antarctic scale and for the 6 regions outlined in Fig. 1: Weddell (from the tip of the Antarctic Peninsula up to ~ 10°S), Indian Ocean (grouping Eastern Weddell and the Indian Ocean ice shelves except Amery ice shelf), Western Pacific (with Amery ice shelf included), Bellingshausen, Amundsen (the eastern Ross Sea grouped with the Amundsen ice shelves) and Ross (the Ross ice shelf cavity on its own). Variables analyzed include ice-shelf basal melt rate, ocean temperature and salinity (both in the open ocean and inside the ice-shelf cavities), sea-ice extent, ocean surface stress (total stress absorbed by the surface of the ocean, i.e. the combination of wind- and sea-ice-induced surface stresses weighted by the sea-ice concentration), maximum vertical velocity (representative of upwelling), winter (JJA) mixed layer depth and along-slope geostrophic velocity at the continental shelf break (used to represent the slope current intensity). Ocean thermodynamical properties are expressed with the TEOS-10 standard[100] (i.e., conservative temperature and absolute salinity). The changes between SAM-perturbed experiments and the CTRL experiment are analyzed (vs. the mean values), either as time series over the 30-year period or averaged over years 25 to 29. Diagnostics consist of spatially-averaged values and time series, maps, vertical sections along the ice-shelf front or along the continental shelf break, cross sections across ice shelves and depth vs. time plots. Ninety-five percent confidence intervals are indicated where applicable by calculating the standard deviation of the values of all grid points within a given ice shelf, region or the whole Antarctic. Statistical significance of changes is evaluated based on a two-sided t-test, with a null hypothesis of zero change.

Comparison with satellite-derived measurements. To put the ice-shelf basal melt rate changes we obtain into perspective, we provide a rough comparison with satellite-derived measurements of the rates of the Antarctic ice-sheet (AIS) mass change over the period 1992–2011 (-76 ± 59 Gt yr^{-1}), 1992–2017 (-109 ± 56 Gt yr^{-1})[3], and with the excess ice-shelf meltwater flux over 1994–2018 (160 ± 150 Gt yr^{-1}, compared to steady state)[59]. Based on the SAM index change over those time periods[101], i.e. +0.2 standard deviation for the period 1992–2011, +0.7 standard deviation for 1992–2017 and +0.8 standard deviation for 1994–2018, we estimate the proportion of these observed changes that could be explained by changes in the SAM. We find that the intensification of the SAM could explain about one tenth, one quarter and one fifth of, respectively, the AIS mass change over 1992–2011, the AIS mass change over 1992–2017 and the excess meltwater flux estimated over 1994–2018 (see the Results and Discussion section).

Data availability

The input datasets used for reproducing the results found in this study are publicly available on Zenodo[102].

Due to their prohibitive size, model outputs are only available upon request to the corresponding author.

The Marshall (2003)[101] SAM index was downloaded on March 3rd, 2021 from https://legacy.bas.ac.uk/met/gjma/sam.html. The Abram et al. (2014)[20] SAM 1000 Year Reconstruction was downloaded from https://www.ncei.noaa.gov/access/paleo-search/study/16197on November 3rd, 2021. The ERA5 data[97,103] was downloaded on September 1st, 2019 from the Copernicus Climate Change Service (C3S) Climate Data Store. The results contain modified Copernicus Climate Change Service information 2020. Neither the European Commission nor ECMWF is responsible for any use that may be made of the Copernicus information or data it contains. The ORAS5 data[99] was downloaded on September 1st, 2019 from the Integrated Climate Data Center hosted at Universität Hamburg (https://www.cen.uni-hamburg.de/en/icdc/data/ocean/easy-init-ocean/ecmwf-oras5.html).

Code availability

The full NEMO sources used for reproducing the results found in this study are publicly available on Zenodo[104]. All figures were created with the Matplotlib[105] and Cartopy[106] Python libraries. Most of the analyses also rely on the NCO and CDO[107] softwares.

Received: 26 November 2021; Accepted: 16 May 2022;
Published online: 22 June 2022

References

1. IPCC. Climate Change 2021: The Physical Science Basis. Contribution of Working Group I to the Sixth Assessment Report of the Intergovernmental Panel on Climate Change [Masson-Delmotte, V., P. Zhai, A. Pirani, S.L. Connors, C. Péan, S. Berger, N. Caud, Y. Chen, L. Goldfarb, M. I. Gomis, M. Huang, K. Leitzell, E. Lonnoy, J.B.R. Matthews, T. K. Maycock, T. Waterfield, O. Yelekçi, R. Yu and B. Zhou (eds.)]. *Cambridge University Press* 3949 pp. (in press). https://www.ipcc.ch/report/ar6/wg1 (last access: March 7th, 2022).
2. Meredith, M. et al. Polar Regions. In Pörtner, H.-O. et al. (eds.) IPCC Special Report on the Ocean and Cryosphere in a Changing Climate (Intergovernmental Panel on Climate Change, 2019). https://www.ipcc.ch/srocc/chapter/chapter-3-2/ (last access: March 7th, 2022).
3. IMBIE team. Mass balance of the Antarctic Ice Sheet from 1992 to 2017. *Nature* **558**, 219-222 (2018).

4. Rignot, E. et al. Four decades of Antarctic Ice Sheet mass balance from 1979–2017. *Proc. Natl. Acad. Sci. U.S.A.* **116**, 1095–1103 (2019).
5. Dutrieux, P. et al. Strong sensitivity of Pine Island ice-shelf melting to climatic variability. *Science* **343**, 174–178 (2014).
6. Jenkins, A. et al. West Antarctic Ice Sheet retreat in the Amundsen Sea driven by decadal oceanic variability. *Nat. Geosci.* **11**, 733–738 (2018).
7. Holland, P. R., Bracegirdle, T. J., Dutrieux, P., Jenkins, A. & Steig, E. J. West Antarctic ice loss influenced by internal climate variability and anthropogenic forcing. *Nat. Geosci.* **12**, 718–724 (2019).
8. Kusahara, K. Interannual-to-multidecadal responses of Antarctic ice shelf–ocean interaction and coastal water masses during the twentieth century and the early twenty-first century to dynamic and thermodynamic forcing. *J. Clim.* **33**, 4941–4973 (2020).
9. Holland, P. R. The seasonality of Antarctic sea ice trends. *Geophys. Res. Lett.* **41**, 4230–4237 (2014).
10. Ludescher, J., Yuan, N. & Bunde, A. Detecting the statistical significance of the trends in the Antarctic sea ice extent: an indication for a turning point. *Clim. Dyn.* **53**, 237–244 (2019).
11. Thompson, D. W. et al. Signatures of the Antarctic ozone hole in Southern Hemisphere surface climate change. *Nat. Geosci.* **4**, 741–749 (2011).
12. Merino, N. et al. Impact of increasing Antarctic glacial freshwater release on regional sea-ice cover in the Southern Ocean. *Ocean Model.* **121**, 76–89 (2018).
13. Holland, P. R. et al. Oceanic and atmospheric forcing of Larsen C Ice-Shelf thinning. *Cryosphere* **9**, 1005–1024 (2015).
14. Meehl, G. A. et al. Sustained ocean changes contributed to sudden Antarctic sea ice retreat in late 2016. *Nature Comm.* **10**, 1–9 (2019).
15. Zunz, V., Goosse, H. & Massonnet, F. How does internal variability influence the ability of CMIP5 models to reproduce the recent trend in Southern Ocean sea ice extent? *Cryosphere* **7**, 451–468 (2013).
16. Wang, C., Zhang, L., Lee, S.-K., Wu, L. & Mechoso, C. R. A global perspective on CMIP5 climate model biases. *Nat. Clim. Change* **4**, 201–205 (2014).
17. Agosta, C., Fettweis, X. & Datta, R. Evaluation of the CMIP5 models in the aim of regional modelling of the Antarctic surface mass balance. *Cryosphere* **9**, 2311–2321 (2015).
18. Jones, J. M. et al. Assessing recent trends in high-latitude Southern Hemisphere surface climate. *Nat. Clim. Change* **6**, 917–926 (2016).
19. Pattyn, F. et al. The Greenland and Antarctic ice sheets under 1. 5°C global warming. *Nat. Clim. Change* **8**, 1053–1061 (2018).
20. Abram, N. J. et al. Evolution of the Southern Annular Mode during the past millennium. *Nat. Clim. Change* **4**, 564–569 (2014).
21. Dätwyler, C. et al. Teleconnection stationarity, variability and trends of the Southern Annular Mode (SAM) during the last millennium. *Clim. Dyn.* **51**, 2321–2339 (2018).
22. Thompson, D. W. & Wallace, J. M. Annular modes in the extratropical circulation. Part I: Month-to-month variability. *J. Clim* **13**, 1000–1016 (2000).
23. Marshall, G. J., Orr, A. & Turner, J. A predominant reversal in the relationship between the SAM and East Antarctic temperatures during the twenty-first century. *J. Clim* **26**, 5196–5204 (2013).
24. Fogt, R. L. & Marshall, G. J. The Southern annular mode: Variability, trends, and climate impacts across the Southern Hemisphere. *Wiley Interdiscip. Rev. Clim. Change* **11**, e652 (2020).
25. Perren, B. B. et al. Southward migration of the Southern Hemisphere westerly winds corresponds with warming climate over centennial timescales. *Commun. Earth Environ.* **1**, 1–8 (2020).
26. Goyal, R., Sen Gupta, A., Jucker, M. & England, M. H. Historical and projected changes in the Southern Hemisphere surface westerlies. *Geophys. Res. Lett.* **48**, e2020GL090849 (2021).
27. Lefebvre, W., Goosse, H., Timmermann, R. & Fichefet, T. Influence of the Southern Annular Mode on the sea ice–ocean system. *J. Geophys. Res. Oceans* **109**, C09005 (2004).
28. Lefebvre, W. & Goosse, H. Influence of the Southern Annular Mode on the sea ice-ocean system: the role of the thermal and mechanical forcing. *Ocean Sci.* **1**, 145–157 (2005).
29. Purich, A., Cai, W., England, M. H. & Cowan, T. Evidence for link between modelled trends in Antarctic sea ice and underestimated westerly wind changes. *Nature Comm.* **7**, 1–9 (2016).
30. Turner, J., Hosking, J. S., Marshall, G. J., Phillips, T. & Bracegirdle, T. J. Antarctic sea ice increase consistent with intrinsic variability of the Amundsen Sea Low. *Clim. Dyn.* **46**, 2391–2402 (2016).
31. Blanchard-Wrigglesworth, E., Roach, L. A., Donohoe, A. & Ding, Q. Impact of winds and Southern Ocean SSTs on Antarctic sea ice trends and variability. *J. Clim.* **34**, 949–965 (2021).
32. Doddridge, E. W., Marshall, J., Song, H., Campin, J.-M. & Kelley, M. Southern Ocean heat storage, reemergence, and winter sea ice decline induced by summertime winds. *J. Clim.* **34**, 1403–1415 (2021).
33. Medley, B. & Thomas, E. Increased snowfall over the Antarctic Ice Sheet mitigated twentieth-century sea-level rise. *Nature Clim. Change* **9**, 34–39 (2019).
34. Dalaiden, Q., Goosse, H., Lenaerts, J. T., Cavitte, M. G. & Henderson, N. Future Antarctic snow accumulation trend is dominated by atmospheric synoptic-scale events. *Commun. Earth Environ.* **1**, 1–9 (2020).
35. Wille, J. D. et al. Antarctic atmospheric river climatology and precipitation impacts. *J. Geophys. Res. Atmos.* **126**, e2020JD033788 (2021).
36. Spence, P. et al. Rapid subsurface warming and circulation changes of Antarctic coastal waters by poleward shifting winds. *Geophys. Res. Lett.* **41**, 4601–4610 (2014).
37. Donat-Magnin, M. et al. Ice-shelf melt response to changing winds and glacier dynamics in the Amundsen Sea sector, Antarctica. *J. Geophys. Res. Oceans* **122**, 10206–10224 (2017).
38. Spence, P. et al. Localized rapid warming of West Antarctic subsurface waters by remote winds. *Nature Clim. Change* **7**, 595–603 (2017).
39. Lin, X. & Wang, Z. Simulated impact of Southern Hemisphere westerlies on Antarctic Continental Shelf Bottom Water temperature. *Adv. Polar Sci.* **29**, 3–19 (2018).
40. Fogt, R. L. et al. Historical SAM variability. Part II: Twentieth-century variability and trends from reconstructions, observations, and the IPCC AR4 models. *J. Clim.* **22**, 5346–5365 (2009).
41. Thompson, D. W. & Solomon, S. Interpretation of recent Southern Hemisphere climate change. *Science* **296**, 895–899 (2002).
42. Fyfe, J. C., Saenko, O. A., Zickfeld, K., Eby, M. & Weaver, A. J. The role of poleward-intensifying winds on Southern Ocean warming. *J. Clim* **20**, 5391–5400 (2007).
43. Bracegirdle, T. J. et al. Assessment of surface winds over the Atlantic, Indian, and Pacific Ocean sectors of the Southern Ocean in CMIP5 models: Historical bias, forcing response, and state dependence. *J. Geophys. Res. Atmos.* **118**, 547–562 (2013).
44. Zheng, F., Li, J., Clark, R. T. & Nnamchi, H. C. Simulation and projection of the Southern Hemisphere annular mode in CMIP5 models. *J. Clim.* **26**, 9860–9879 (2013).
45. Bracegirdle, T. J. et al. Twenty first century changes in Antarctic and Southern Ocean surface climate in CMIP6. *Atmos. Sci. Lett.* **21**, e984 (2020).
46. Purich, A. & England, M. H. Historical and future projected warming of antarctic shelf bottom water in CMIP6 models. *Geophys. Res. Lett.* **48**, e2021GL092752 (2021).
47. Purich, A., Cowan, T., Min, S.-K. & Cai, W. Autumn precipitation trends over Southern Hemisphere midlatitudes as simulated by CMIP5 models. *J. Clim.* **26**, 8341–8356 (2013).
48. Zambri, B., Solomon, S., Thompson, D. W. & Fu, Q. Emergence of Southern Hemisphere stratospheric circulation changes in response to ozone recovery. *Nature Geosci.* **14**, 638–664 (2021).
49. Webb, D., Holmes, R., Spence, P. & England, M. Barotropic Kelvin wave-induced bottom boundary layer warming along the West Antarctic Peninsula. *J. Geophys. Res.: Oceans* **124**, 1595–1615 (2019).
50. Timmermann, R., Beckmann, A. & Hellmer, H. Simulations of ice-ocean dynamics in the Weddell Sea 1. Model configuration and validation. *J. Geophys. Res. Oceans* **107**, 10–1 (2002).
51. Timmermann, R., Wang, Q. & Hellmer, H. Ice-shelf basal melting in a global finite-element sea-ice/ice-shelf/ocean model. *Ann. Glaciol.* **53**, 303–314 (2012).
52. Mathiot, P., Jenkins, A., Harris, C. & Madec, G. Explicit representation and parametrised impacts of under ice shelf seas in the z* coordinate ocean model NEMO 3.6. *Geosci. Model Dev.* **10**, 2849–2874 (2017).
53. Storkey, D. et al. UK Global Ocean GO6 and GO7: A traceable hierarchy of model resolutions. *Geosci. Model Dev.* **11**, 3187–3213 (2018).
54. Jeong, H. et al. Impacts of ice-shelf melting on water-mass transformation in the Southern Ocean from E3SM simulations. *J. Clim* **33**, 5787–5807 (2020).
55. Richter, O., Gwyther, D. E., King, M. A. & Galton-Fenzi, B. K. The impact of tides on Antarctic ice shelf melting. *Cryosphere.* **16**, 1409–1429 (2022).
56. Reese, R., Gudmundsson, G. H., Levermann, A. & Winkelmann, R. The far reach of ice-shelf thinning in Antarctica. *Nature Climate Change* **8**, 53–57 (2018).
57. Rousset, C. et al. The Louvain-La-Neuve sea ice model LIM3.6: Global and regional capabilities. *Geosci. Model Dev.* **8**, 2991–3005 (2015).
58. Madec, G. et al. NEMO ocean engine. Tech. Rep., Insitut Pierre-Simon Laplace (2017).
59. Adusumilli, S., Fricker, H. A., Medley, B., Padman, L. & Siegfried, M. R. Interannual variations in meltwater input to the southern ocean from antarctic ice shelves. *Nature Geosci.* **13**, 616–620 (2020).
60. Holland, D. M., Jacobs, S. S. & Jenkins, A. Modelling the ocean circulation beneath the Ross Ice Shelf. *Antarctic Science* **15**, 13–23 (2003).
61. Joughin, I. & Padman, L. Melting and freezing beneath Filchner-Ronne Ice Shelf, Antarctica. *Geophys. Res. Lett.* **30** (2003).
62. Rignot, E., Jacobs, S., Mouginot, J. & Scheuchl, B. Ice-shelf melting around Antarctica. *Science* **341**, 266–270 (2013).
63. Lewis, E. L. & Perkin, R. G. Ice pumps and their rates. *J. Geophys. Res.: Oceans* **91**, 11756–11762 (1986).

64. Holland, M. M., Landrum, L., Kostov, Y. & Marshall, J. Sensitivity of Antarctic sea ice to the Southern Annular Mode in coupled climate models. *Clim. Dyn.* **49**, 1813–1831 (2017).
65. Seviour, W. J. M. et al. The Southern Ocean sea surface temperature response to ozone depletion: A multimodel comparison. *J. Clim.* **32**, 5107–5121 (2019).
66. Rackow, T. et al. Delayed Antarctic sea-ice decline in high-resolution climate change simulations. *Nat. Comm.* **13** https://doi.org/10.1038/s41467-022-28259-y (2022).
67. Dufour, C. O. et al. Standing and transient eddies in the response of the Southern Ocean meridional overturning to the Southern Annular Mode. *J. Clim.* **25**, 6958–6974 (2012).
68. Doddridge, E. W. et al. Eddy compensation dampens Southern Ocean sea surface temperature response to westerly wind trends. *Geophys. Res. Lett.* **46**, 4365–4377 (2019).
69. Li, Q., England, M. H. & Hogg, A. Mc. C. Transient Response of the Southern Ocean to Idealized Wind and Thermal Forcing across Different Model Resolutions. *J. Clim.* **34**, 5477–5496 (2021).
70. Kohyama, T. & Hartmann, D. L. Antarctic sea ice response to weather and climate modes of variability. *J. Clim.* **29**, 721–741 (2016).
71. Polvani, L. et al. Interannual SAM modulation of Antarctic sea ice extent does not account for its long-term trends, pointing to a limited role for ozone depletion. *Geophys. Res. Lett.* 2021GL094871 (2021).
72. Raphael, M. N. et al. The Amundsen Sea low: Variability, change, and impact on Antarctic climate. *Bull. Amer. Meteor. Soc.* **97**, 111–121 (2016).
73. Michel, R., Linick, T. & Williams, P. Tritium and carbon-14 distributions in seawater from under the Ross Ice Shelf Project ice hole. *Science* **203**, 445–446 (1979).
74. Nicholls, K. W. & Østerhus, S. Interannual variability and ventilation timescales in the ocean cavity beneath Filchner-Ronne Ice Shelf, Antarctica. *J. Geophys. Res. Oceans* **109** (2004).
75. Naughten, K. A. et al. Modeling the influence of the Weddell Polynya on the Filchner–Ronne Ice Shelf Cavity. *J. Clim* **32**, 5289–5303 (2019).
76. Naughten, K. A. et al. Two-timescale response of a large Antarctic ice shelf to climate change. *Nat. Comm.* **12**, 1–10 (2021).
77. Ferreira, D., Marshall, J., Bitz, C. M., Solomon, S. & Plumb, A. Antarctic Ocean and sea ice response to ozone depletion: A two-time-scale problem. *J. Clim* **28**, 1206–1226 (2015).
78. Cook, A. J. et al. Ocean forcing of glacier retreat in the western Antarctic Peninsula. *Science* **353**, 283–286 (2016).
79. Naughten, K. A. et al. Simulated twentieth-century ocean warming in the Amundsen Sea, West Antarctica. *Geophys. Res. Lett.* 2021GL094566 (2022).
80. Turner, J., Phillips, T., Hosking, J. S., Marshall, G. J. & Orr, A. The Amundsen Sea low. *Int. J. Climatol.* **33**, 1818–1829 (2013).
81. Holland, M. M., Landrum, L., Raphael, M. N. & Kwok, R. The regional, seasonal, and lagged influence of the Amundsen sea low on Antarctic sea ice. *Geophys. Res. Lett.* **45**, 11–227 (2018).
82. Dotto, T. S. et al. Control of the oceanic heat content of the Getz-Dotson Trough, Antarctica, by the Amundsen Sea Low. *J. Geophys. Res. Oceans* **125**, e2020JC016113 (2020).
83. Thomas, E. R. & Abram, N. J. Ice core reconstruction of sea ice change in the Amundsen-Ross Seas since 1702 AD. *Geophys. Res. Lett.* **43**, 5309–5317 (2016).
84. Dalaiden, Q., Goosse, H., Rezsohazy, J. & Thomas, E. R. Reconstructing atmospheric circulation and sea-ice extent in the West Antarctic over the past 200 years using data assimilation. *Clim. Dyn.* **57**, 3479–3503 (2021).
85. Thompson, A. F., Stewart, A. L., Spence, P. & Heywood, K. J. The Antarctic slope current in a changing climate. *Rev. Geophys.* **56**, 741–770 (2018).
86. Nakayama, Y. et al. Antarctic slope current modulates ocean heat intrusions towards Totten glacier. *Geophys. Res. Lett.* **48**, e2021GL094149 (2021).
87. Nakayama, Y., Timmermann, R., Rodehacke, C. B., Schröder, M. & Hellmer, H. H. Modeling the spreading of glacial meltwater from the Amundsen and Bellingshausen Seas. *Geophys. Res. Lett.* **41**, 7942–7949 (2014).
88. Golledge, N. R. et al. Global environmental consequences of twenty-first-century ice-sheet melt. *Nature* **566**, 65–72 (2019).
89. Timmermann, R. & Hellmer, H. H. Southern Ocean warming and increased ice shelf basal melting in the twenty-first and twenty-second centuries based on coupled ice-ocean finite-element modelling. *Ocean Dynamics* **63**, 1011–1026 (2013).
90. Morlighem, M. et al. Deep glacial troughs and stabilizing ridges unveiled beneath the margins of the Antarctic ice sheet. *Nature Geosci.* **13**, 132–137 (2020).
91. NOAA National Geophysical Data Center. ETOPO1 1 arc-minute global relief model. Dataset. NCEI Metadata ID gov.noaa.ngdc.mgg.dem:316, accessed March 7th, 2022.
92. Amante, C. & Eakins, B. W. ETOPO1 arc-minute global relief model: procedures, data sources and analysis. Tech. Rep., National Center for Atmospheric Research (2009).
93. Pattyn, F. Sea-level response to melting of Antarctic ice shelves on multi-centennial timescales with the fast Elementary Thermomechanical Ice Sheet model (f.ETISh v1.0). *Cryosphere* **11**, 1851–1878 (2017).
94. Pelletier, C. et al. PARASO, a circum-Antarctic fully coupled ice-sheet–ocean–sea-ice–atmosphere–land model involving f.ETISh1.7, NEMO3.6, LIM3.6, COSMO5.0 and CLM4.5. *Geosci. Model Dev.* **15**, 553–594 (2022).
95. Jourdain, N. C., Merino, N., Le Sommer, J., Durand, G. & Mathiot, P. Interannual iceberg meltwater fluxes over the Southern Ocean https://doi.org/10.5281/zenodo.3514728 (2019).
96. Large, W. G. & Yeager, S. G. Diurnal to Decadal Global Forcing For Ocean and Sea-Ice Models: The Data Sets and Flux Climatologies. Tech. Rep., National Center for Atmospheric Research (2004). https://doi.org/10.5065/D6KK98Q6.
97. Hersbach, H. et al. The ERA5 global reanalysis. *Q. J. R. Meteorol. Soc.* **146**, 1999–2049 (2020).
98. Stewart, K. et al. JRA55-do-based repeat year forcing datasets for driving ocean–sea-ice models. *Ocean Model.* **147**, 101557 (2020).
99. Zuo, H., Balmaseda, M. A., Tietsche, S., Mogensen, K. & Mayer, M. The ECMWF operational ensemble reanalysis–analysis system for ocean and sea ice: a description of the system and assessment. *Ocean Sci.* **15** (2019).
100. IOC. The International thermodynamic equation of seawater–2010: calculation and use of thermodynamic properties. Tech. Rep., UNESCO (2010). https://doi.org/10.25607/OBP-1338.
101. Marshall, G. J. Trends in the Southern annular mode from observations and reanalyses. *J. Clim* **16**, 4134–4143 (2003).
102. Verfaillie, D. & Pelletier, C. Input dataset related to NEMO circum-Antarctic configuration for SAM sensitivity tests https://doi.org/10.5281/zenodo.5780039 (2021).
103. Hersbach, H. et al. ERA5 hourly data on single levels from 1979 to present (2018). Dataset. Retrieved September 1st, 2019.
104. Pelletier, C. & Verfaillie, D. NEMO circum-Antarctic configuration for SAM sensitivity tests https://doi.org/10.5281/zenodo.5780018 (2021).
105. Hunter, J. D. Matplotlib: A 2D graphics environment. *Comput. Sci. Eng.* **9**, 90–95 (2007).
106. Met Office. Cartopy: a cartographic python library with a Matplotlib interface. Exeter, Devon, https://scitools.org.uk/cartopy (2010–2015).
107. Schulzweida, U. Cdo user's guide. https://doi.org/10.5281/zenodo.3539275 (2019).

Acknowledgements

This work was funded through the PARAMOUR project "Decadal predictability and variability of polar climate: the role of atmosphere-ocean-cryosphere multiscale interactions" supported by the Fonds de la Recherche Scientifique-FNRS under Grant number O0100718F (EOS ID 30454083). C.B. and N.J. are supported by the European Union's Horizon 2020 research and innovation programme under grant agreement no. 820575 (TiPACCs). J.W. and V.F. acknowledge support from the Agence Nationale de la Recherche project ANR-20-CE01-0013 (ARCA).

Computational resources have been provided by the supercomputing facilities of the Université catholique de Louvain (CISM/UCL) and the Consortium des Équipements de Calcul Intensif en Fédération Wallonie Bruxelles (CÉCI) funded by the Fond de la Recherche Scientifique de Belgique (F.R.S.-FNRS) under convention 2.5020.11 and by the Walloon Region. The present research also benefited from computational resources made available on the Tier-1 supercomputer of the Fédération Wallonie-Bruxelles, infrastructure funded by the Walloon Region under the grant agreement n°1117545.

We would like to thank Lars Zipf, Konstanze Haubner and Frank Pattyn (Université Libre de Bruxelles, Belgium) for providing the ice-sheet geometry used in these experiments. Finally, we thank the editor and the two reviewers for constructive comments and suggestions that helped us greatly improve our manuscript.

Author contributions

H.G. and D.V. designed the research. Guidance on ocean and ice-shelf diagnostics was provided by N.J., C.P. and C.B. V.F., J.W. and Q.D. brought their expertise concerning ice-sheet atmosphere interactions, while expertise on sea ice was provided by T.F. and H.G. D.V. and C.P. prepared the numerical experiments, diagnostics and figures. D.V. performed the analysis, wrote the initial draft and coordinated the manuscript preparation with input from all authors.

Competing interests

The authors declare no competing interests.

Additional information

Supplementary information The online version contains supplementary material available at https://doi.org/10.1038/s43247-022-00458-x.

Correspondence and requests for materials should be addressed to Deborah Verfaillie.

Peer review information *Communications Earth & Environment* thanks the anonymous reviewers for their contribution to the peer review of this work. Primary Handling Editors: Heike Langenberg. Peer reviewer reports are available.